LASER & PHOTONICS REVIEWS
www.lpr-journal.org

Asymmetric Domain Growth for Bistable Information Hiding and Revealing in Blue Phase Liquid Crystals

Quanming Chen, Cheng Ouyang, Zhiyao Xie, Chunting Xu, Zongxuan Wu, Jiayuan Min, Yanjun Liu, Dan Luo, and Wei Hu**

Photonic crystals (PCs) are innovative structures with periodic variations in refractive index, enabling remarkable light manipulation capabilities that hold promise for fundamental research and practical applications in physics, biology, and engineering. This work explores the hierarchical structures of blue-phase liquid crystals (BPLCs), which are characterized by distinct omnidirectional photonic band gaps. By leveraging the asymmetric domain growth of BP a novel method for bistable information hiding and revealing is proposed. With a single-side photopatterned cell, a polydomain of BPLC is formed during cooling thanks to the generated temperature gradient. Upon applying an alternating current (AC) electric field, a monodomain state is achieved, allowing for clear, high-contrast information retrieval. Both quick response (QR) code and geometric phase hologram are encoded to the alignment layer, and reversible information hiding and revealing are demonstrated via alternating the heating and electric driving processes. Moreover, continuous shifting of reflective color is presented via varying applied voltages. The proposed technique may inspire future applications in optical encryption, camouflage, and advanced information security technologies.

1. Introduction

Photonic crystal (PC), due to its powerful capability in light manipulation, offers a promising platform for both fundamental research and versatile applications across physics,[1] biology,[2] and engineering.[3] It is characterized by a periodic variation in refractive indices with a periodicity of hundreds of nanometers and thus leads to an intrinsic photonic band gap (PBG) corresponding to specific color reflection.[4] PCs widely exist in nature, such as opals,[5] wings of Menelaus morphos,[6] peacock tail feathers,[7] and viruses.[8] Actively controllable PCs benefit living beings in terms of camouflage, courtships, and communications. A classic example is that via manipulation of PCs inside their skin, chameleons actively tune their color to match the surroundings, thereby avoiding hunting from predators.[9] Various artificial PCs have been developed to mimic the above functions. PCs can be prepared via standard nanofabrication procedures but suffer from time- and cost-consuming fabrication and static functions. The self-assembly of soft matter is more favorable because of its cost-effective and scalable production as well as excellent stimulus responsiveness. Colloids,[10] polymers[11] and liquid crystals (LCs)[12] are typical soft materials. Among them, LC PCs have attracted intensive attention because of their rich self-assembled structures and sensitivity to various external fields.[13] A cholesteric LC is a 1D helical PC. Its helical pitch and even helicity can be varied by stress,[14] heat,[15] electricity,[16] and light,[17] resulting in impressive wavelength shifting and spin reversing of light.[18] Usually, a maintained external stimulus is required to sustain a specific transformed state, limiting their applications in which bistable information hiding and revealing are needed.

The blue phase liquid crystal (BPLC) consists of a hierarchical 3D configuration. LC molecules self-assemble into double-twisted cylinders (DTCs), which further pack into simple-cubic (BP II) or body-centered-cubic (BP I) lattices.[19] The lattice constants are hundreds of nanometers in size. Thanks to the 3D helical structure, BPLCs exhibit distinctive omnidirectional sharp Bragg reflection in the visible range. As a result, BPLCs based optical camouflage,[20] anti-counterfeiting,[21] display[22], and lasing[23] have been intensively investigated. Furthermore, numerical simulation by solving the Maxwell equation reveals that the omnidirectional Bragg reflection is circular polarization (CP) dependent.[24] Specifically, CP of the same handedness as the helicity of BPLCs is selectively reflected, while CP of the reverse handedness transmits directly. The unique properties promise BPLC great potential in optics and photonics. However, it highly relies on the uniformity of BPLC lattice.

Q. Chen, Z. Wu, J. Min, Y. Liu, D. Luo
Department of Electrical & Electronic Engineering
Southern University of Science and Technology
Shenzhen 518055, China
E-mail: luod@sustech.edu.cn

Q. Chen, C. Ouyang, Z. Xie, C. Xu, W. Hu
National Laboratory of Solid State Microstructures
Jiangsu Physical Science Research Center
College of Engineering and Applied Sciences
Nanjing University
Nanjing 210023, China
E-mail: huwei@nju.edu.cn

The ORCID identification number(s) for the author(s) of this article can be found under https://doi.org/10.1002/lpor.202401635

DOI: 10.1002/lpor.202401635

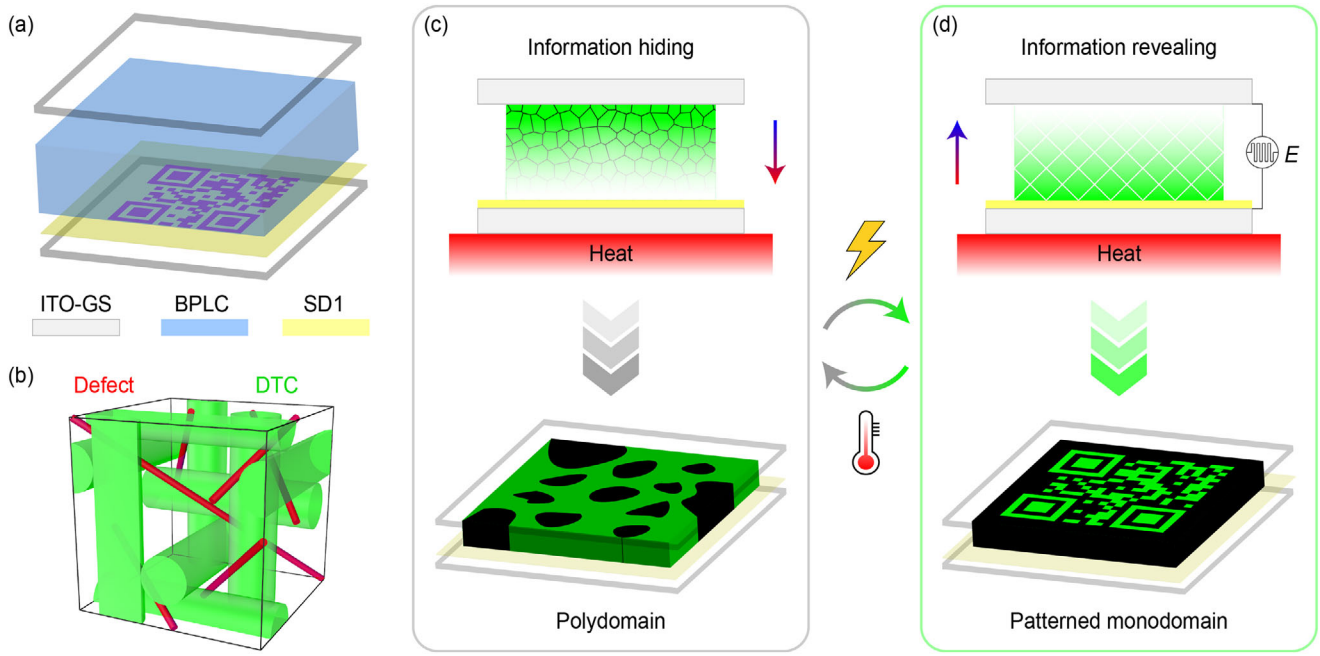

Figure 1. a) LC cell configuration with asymmetric alignments. b) Scheme for the body-centered-cubic lattice of BP I. Schematic illustrations of the asymmetric domain growth of the BPLC and corresponding information c) hiding and d) revealing.

Various physical fields, such as long-lasting electricity,[25] surface acoustic waves,[26] and temperature gradient,[27] have been adopted to drastically enlarge the monodomain size. In addition, alignment,[28] especially photoalignment, supplies an effective strategy to locally guide the domain growth.[29] That means photopatterned alignment spatially defines the lattice orientation of BP domains and thus introduces a Bragg–Berry (BB) phase to the reflected light. By this means, an omnidirectional CP selective hologram is achieved via programming the lattice orientations.[24,30] Recently, a multi-channel holography based on stacked BPLCs was presented based on the CP selective narrowband Bragg reflection.[31] BPLC provides an integrated platform for multidegree light modulation. If one can freely alternate between the patterned monocrystalline domain and randomly orientated multidomain, bistable information hiding and revealing would be accomplished based on the BPLC, which will drastically promote the development of active PCs based optics and photonics.

We propose a hiding and revealing bistable information system based on the asymmetric domain growth of BP I. Only the bottom substrate of the LC cell is photopatterned, while the top substrate is left untreated. During cooling from the isotropic state, a temperature gradient is generated inside the cell; thus, random nucleation first occurs upon the top substrate. As a result, BP I polydomain is formed. After a saturated alternating current (AC) electrical field is applied for 60 s, the patterned BP I monodomain is generated from the homeotropic state. In this process, the crystal growth is dominated by the bottom substrate. Correspondingly, information hiding and revealing can be reversibly transformed by alternating heating and electrical driving. Owing to the rewritability of the photoalignment agent, a geometric phase hologram is encoded to the same sample, and its reflection color is continuously shifted by the electrostriction effect. This work supplies a practical technique to regulate the different domain growth of BP I and may inspire versatile applications in optical encryption, camouflage, and other information security techniques.

2. Results and Discussion

2.1. Concept and Principle

The asymmetric domain growth is carried out with a specially designed BPLC cell. As revealed in **Figure** 1a, the cell is formed by two parallel indium-tin-oxide (ITO) glass substrates. The bottom substrate is coated with the photoalignment agent SD1[32] and then photopatterned, while the top substrate is untreated. They are separated by spacers to maintain a uniform cell gap of 8 μm. After the LC mixture has infiltrated, the BP I of the body-centered cubic lattice (Figure 1b) is generated when it has cooled from the isotropic state. As the bottom substrate contacts the heating stage (high temperature) and the top substrate is exposed to air (low temperature), a vertical temperature gradient is formed inside the cell during the cooling process. In this case, nucleation randomly occurs on the interface between the BPLC and the top substrate first, leading to a polydomain texture. As a result, the recorded information is completely hidden (Figure 1c). The procedure for revealing the information is presented in Figure 1d. A saturated AC electrical field is applied to drive the BP I to the homeotropic state. While keeping the state for a while, the LC mixture is heated up to a temperature approaching the phase transition point of BP II-BP I.[31] After the field is removed, LC spontaneously self-assembles into BP I and monodomain is generated over the unidirectionally photopatterned area as the anchoring supplies extra energy to guide the monocrystal growth. Therefore, the patterned alignment guides the generation of a

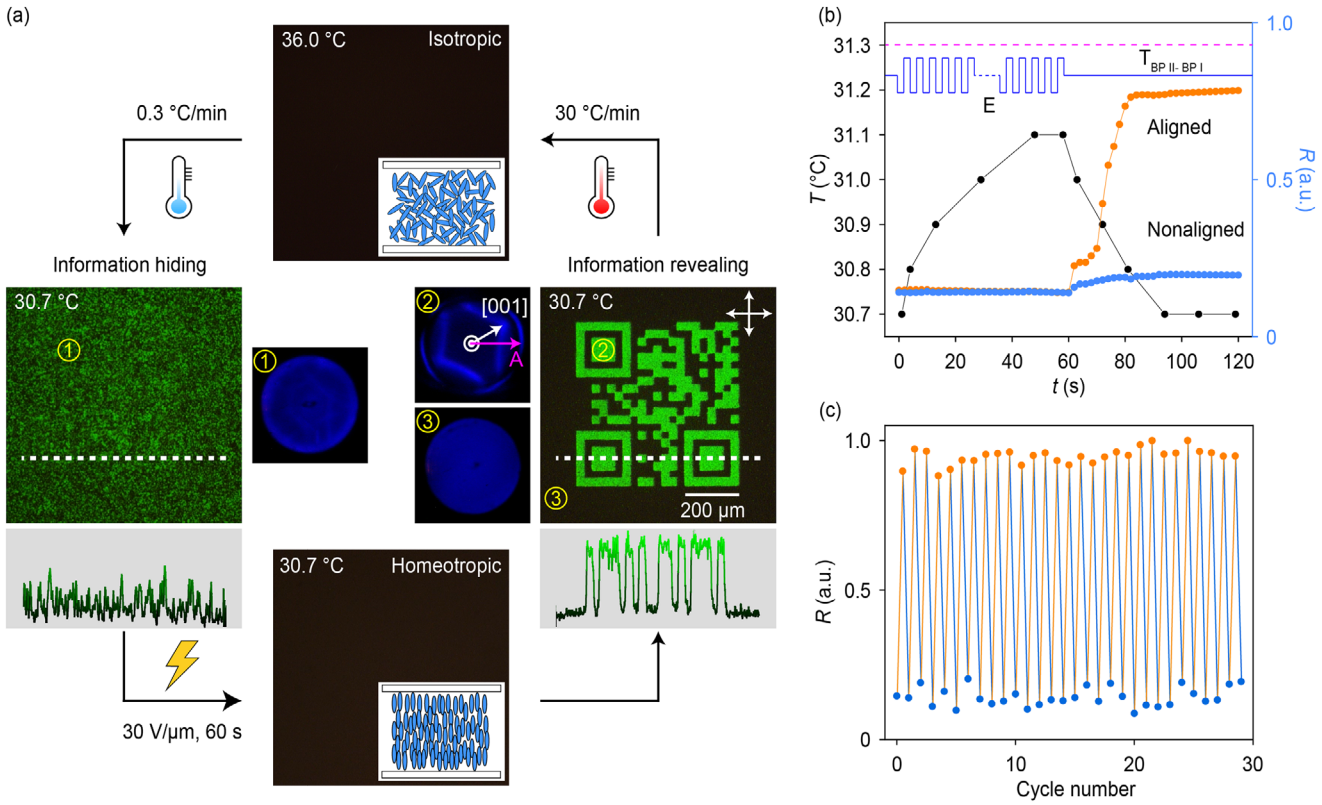

Figure 2. a) Procedure for information hiding and revealing caused by heating or electrical driving. The purple capital letter A indicates the alignment direction in the bottom layer. b) Dependencies of temperature and reflectance on the duration of the applied electric field. The black, orange/blue dashed lines indicate dependencies of temperature and reflectance at the aligned/nonaligned areas on time, respectively. The purple dashed line indicates the BP II–BP I phase transition point (31.3 °C). c) Fatigue resistance test of the information hiding and revealing recycles. The arrows indicate the directions of a pair of crossed polarizers. The scale bar indicates 200 μm for all micrographs.

monodomain with a predesigned shape surrounded by a polydomain over unaligned regions. Owing to the distinct reflectance between the monodomain and the polydomain of BP I, the coded information is clearly revealed. The bistable information hiding and revealing states can be alternated reversibly by heating or electrical driving.

2.2. Bistable Information Hiding and Revealing Based on the Asymmetric Domain Growth of BP I

A quick response (QR) code of "BPLC" is recorded in the alignment layer for a simple demonstration of the above design. As shown in **Figure** 2a, the sample is slowly cooled from the isotropic state (36.0 °C) to BP I (30.7 °C) at a rate of −0.3 °C min^{-1}. The BP I exhibited a polydomain texture, confirmed by the irregular scattering of the Kossel diffraction. Obviously, the encoded information is successfully hidden. Then, an AC electric field of 30 V μm^{-1} is applied to the cell, which drives the LC to the homeotropic state. By applying the voltage for 60 s, the sample is heated to 31.2 °C due to dielectric heating, which approaches the BP II-BP I phase transition point of 31.3 °C (Figure 2b and Figure S1, Supporting Information). After the field is removed, the sample temperature falls back to 30.7 °C within 30 s (the black dashed line). At the same time, the reflectance at the areas with/without alignment treatment increases sharply/negligibly, and then gradually stabilizes within 20 s (the orange/blue dashed lines). As a result, a reflective QR code is clearly observed in high contrast ratio under a polarized optical microscope (POM), due to the large reflectance difference between the photopatterned monodomain and untreated polydomain. The twofold Kossel diagram from the monodomain indicates the lattice orientation of BP $I_{(110)}$.[33] Fixing the alignment direction as the reference axis (indicated by purple letter A, Figure 2a), The angle between the [001] axis and the alignment direction is 28°, which is consistent with double-sided photopatterned cells.[31] In contrast, a blurred Kossel diagram is still observed in unaligned regions, where a polydomain is generated. Therefore, the encoded QR code is clearly revealed. We heated the LC into the isotropic state at a rate of 30 °C min^{-1} to complete a full cycle. The information hiding and revealing states are reversibly alternated via repeating the heating and electrical driving processes. The sample exhibited excellent fatigue resistance; after 30 cycles, the sample still revealed clear and high-contrast QR code as well as a high-quality hiding state (Figure 2c).

2.3. Stability of the Patterned BP I

A series of examinations were carried out to verify the stability of the photopatterned BP I. First, we studied the thermal stability

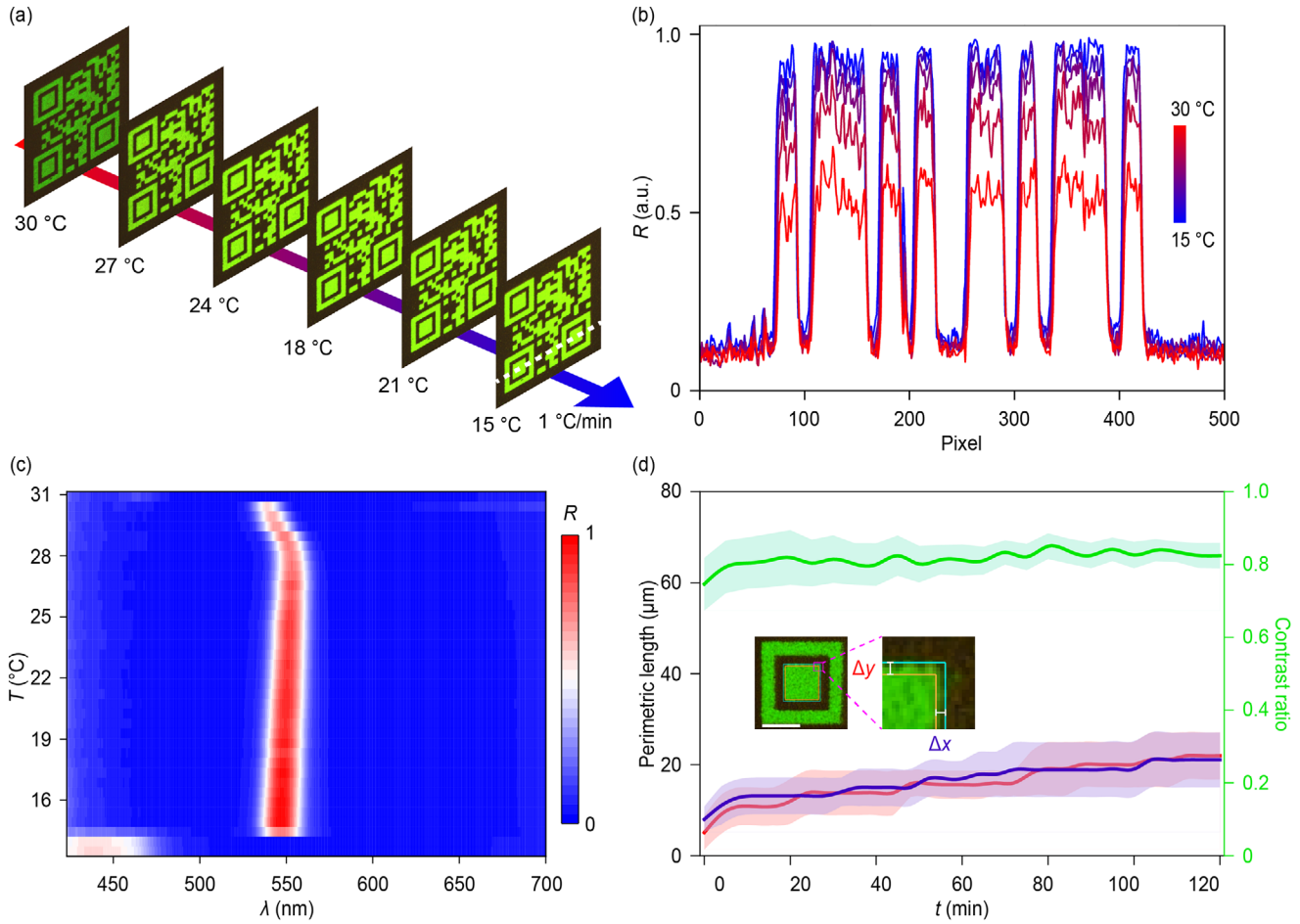

Figure 3. a) Micrographs of the QR code samples at different temperatures, b) corresponding intensity profiles in regions marked by the white dashed line in (a). c) Dependency of central reflection wavelengths on temperature. d) Dependencies of perimetric length and contrast ratio on time. The inset images show the region used for measurement. The scale bar indicates 100 μm.

by varying the temperature in the range of 30.7–15.0 °C. The wide BP I range is attributed to two facts: First, the doped non-mesogenic monomer tends to be trapped into disclination lines of cubic lattices, thus drastically reducing the free energy of the system and broadening the BP range. Second, the alignment layer SD1 provides a strong anchoring, facilitating the stabilization of BP as well. When cooling at a rate of −1 °C min^{-1}, the patterns of both the monodomain and the polydomain remain stable; thus, the QR code maintains excellent visibility (**Figures 3a** and S2, Supporting Information). With decreasing temperature, more regular BP lattices exhibit enhanced reflectance. The above phenomena are also verified by the intensity profiles (Figure 3b), as denoted by the regions marked with white dashed lines. According to the recorded reflection spectra, both the central reflection wavelength (λ_c) and the full width at half maximum (FWHM) remain stable during the temperature variation (Figure 3c). The stability of the QR code during the heating is also confirmed (Figure S3, Supporting Information). Second, the stability with respect to storage time is investigated. The BP I monodomain epitaxially grew in two orthogonal directions synchronously with storage time. The perimetric length eventually increases to ≈20 μm when the sample is held for 120 min (Figure 3d and Figure S4, Supporting Information). The contrast ratio between the aligned and unaligned regions remained steady at an average value of 0.8 (Figure 3d). It is defined as $(I_{max}-I_{min})/(I_{max}+I_{min})$, where I_{max} and I_{min} are the maximum and minimum intensity values, respectively. The above tests suggest the excellent stability of the generated QR code, which is especially meaningful for sustainable usage.

2.4. Geometric Phase Hologram Hiding and Revealing with Variable Colors

Since the information is recorded in the alignment layer and then transferred to the organization of the BP lattice, the information can be dynamically reconfigured via photo rewriting a new pattern in an electrically driven homeotropic state or isotropic state. As mentioned above, the angle between the [001] axis and the alignment direction is fixed at 28°, which means that the lattice orientation can be spatially manipulated by properly setting the alignment direction. We erase the above QR code with unpolarized UV light and rewrite a geometric phase hologram

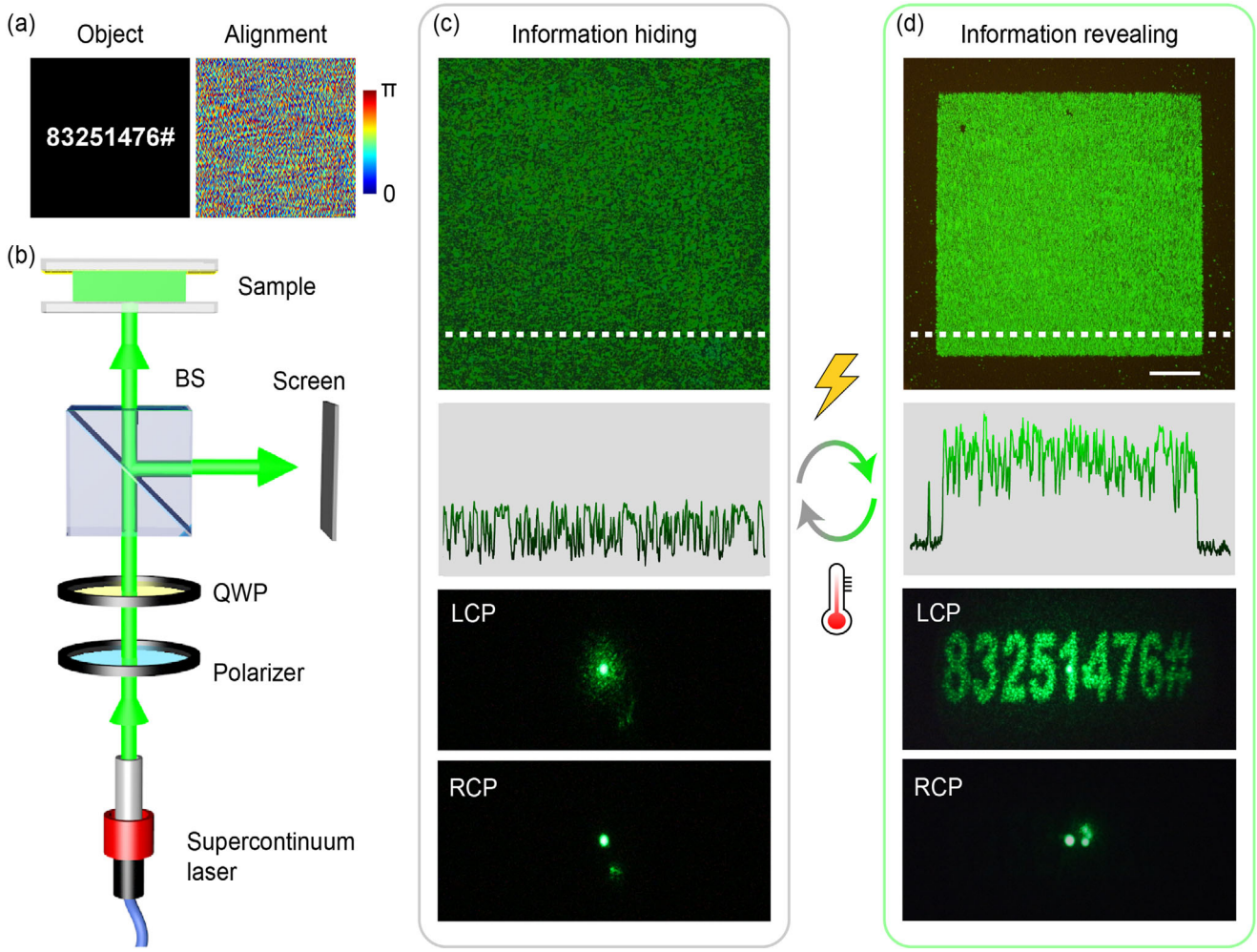

Figure 4. a) Objective far-field diffraction and photoalignment pattern transformed from the corresponding computer-generated hologram. b) Reflective optical setup for holographic characterization. BS: beam splitter, QWP: quarter waveplate. Geometric phase c) hiding and d) revealing states, from top to bottom: POM images, intensity profiles at the regions marked by the white dashed lines, reflections, and diffractions for LCP and RCP incidences at hiding and revealing states, respectively. The scale bar indicates 200 μm for all micrographs.

corresponding to the far-field diffraction of "83251476#" in the homeotropic state via photoalignment (Figure S5, Supporting Information). The alignment direction is transformed from the geometric phase hologram calculated via the Gerchberg–Saxton algorithm (**Figures** 4a and S6, Supporting Information).[34] In our experiments, a reflective optical setup is prepared for holographic characterization. As shown in Figure 4b, the polarization of a supercontinuum laser is controlled by a polarizer and a quarter waveplate (QWP). In the information-hiding state, specular reflections and slight scatterings are received from the polydomain for both left-handed circular polarization (LCP) and right-handed circular polarization (RCP) within the PBG (Figure 4c). In the information-revealing state, the coded far-field information is diffracted for the LCP within the PBG, matching the helicity of the BPLC (Figure 4d). Therefore, both near-field amplitude patterns and far-field geometric phase diffractions are demonstrated. These states can be dynamically reconfigured through photo rewriting and reversibly alternated by heating and electrical driving.

When proper AC signals are applied to a sample, the lattice of BP I extends along the field due to the electrostriction effect.[35] As illustrated in **Figure** 5a, the lattice is elongated along the direction of the electric field (E), which is parallel to [110]. As a result, λ_c redshifts according to the Bragg equation. λ_c increases from 541 to 615 nm as E increases to 15.0 V μm^{-1}. As expected, the color of the sample varies from green to red, and two examples are presented in the insets of Figure 5b. λ_c recovers after E is removed. The far-field diffractions at E values of 7.5 , 10.5, and 15.0 V μm^{-1} are presented in Figure 5c. The encoded information is clearly observed during the whole voltage tuning process; however, the selected colors are different.

Here, information hiding and revealing are carried out based on the asymmetric domain growth of a BP I sample. External fields (heat and electricity) are required only in the switching process, while both states are stable during storage, even for a long time. It is distinctive from conventional strategies, where external stimuli, such as humidity,[36] force,[37] and heat[38] should be maintained to keep the transformed states. This makes the

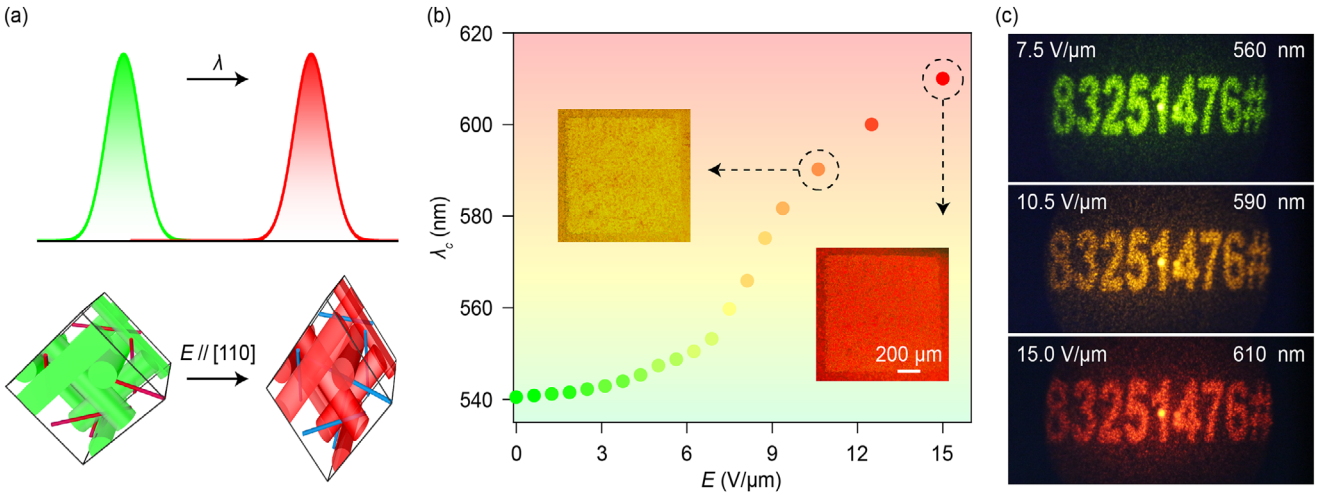

Figure 5. a) Schematic of the wavelength shifting induced by the electrostriction effect of the BP I lattice. b) Dependency of λ_c on E. The insets show micrographs of the samples with λ_c values of 590 and 610 nm. c) Diffraction patterns under electric fields of 7.5, 10.5 and 15.0 V μm^{-1}. The scale bar indicates 200 μm for all micrographs.

technique energy-saving and environmentally friendly. Very recently, an effective strategy to generate large areas and different color monodomains of BP I via reverse electrostriction-directed assembly was presented.[39] In our work, single side alignment is introduced to perform the asymmetric domain growth of BPLC. By leveraging photopatterned alignment and temperature gradience, reversible information hiding and revealing of both near-field QR code patterns and far-field diffraction are demonstrated.

In this work, a hot stage and a voltage generator are adopted for the principle of demonstration to trigger the transition between the information-hiding and revealing states. For practical applications, the hot stage can be replaced by an integrated single-side (adjacent to the alignment layer) ITO heater, while the electric signal is vertically applied to perform the electric stimulus. Since the temperature gradient is kept, the randomly oriented polydomain will be obtained regardless of the initial phase state (isotropic or BP II). The information revealing only works when the electric field is applied at BPI state. We use a mini air conditioner to mimic the variable and complex ambient temperature and find that the accuracy of information degrades at lower ambient temperatures (Figure S7, Supporting Information). This issue is expected to be solved via optimizing the material composition. BP I is adopted instead of BP II because of its better thermal stability. After the electric field is removed, the epitaxial growth of the BP II domain heavily degrades the display quality (Figure S8, Supporting Information). The information can also be obtained by introducing a reversed temperature gradient. The information hiding only occurs when a positive temperature gradient between the unaligned and patterned substrates exists during the phase transition. However, common temperature variations are uniform (with no gradient). In this case, the patterned alignment dominates the crystal growth due to its stronger anchoring energy, thus leading to the information revealing. Moreover, the clearing point of BP can be freely tuned by tailoring the composition, enabling information to be revealed at predesigned temperatures. It supplies a promising strategy for monitoring the temperature of thermosensitive products, such as vaccines during cold chain transportation.

When the asymmetric cell is reversed, monodomain guided by the patterned alignment is obtained in the same cooling process (Figure S9), verifying that the temperature gradient-induced asymmetric nucleation plays a crucial role in information hiding. Polydomain BP I is also observed on the photo-alignment side before applying an electric field (Figure S10, Supporting Information), which further confirms that the nonaligned top substrate guides the random polycrystal growth, thus supplying a full information-hiding state on both sides of the cell. The information hiding and revealing exhibits an excellent robustness in spacing thickness of the single-sided alignment cell (Figure S11, Supporting Information). Gentle cooling is favorable to high-quality information-hiding states, as rapid cooling leads to information leakage due to the simultaneous rapid nucleation from both sides (Figure S12, Supporting Information). Both the information hiding and revealing states are stable since the BP I (15.0 – 30.7 °C) is maintained. It means no heating is required for use at room temperature. Stimuli are only required in the state-switching process; therefore, it is energy-saving. A mapping relationship between the chirality, lattice constant, and azimuthal orientation of the BPLC lattice and the spin angular momentum, wavelength, and geometric phase of light has already been established. Therefore, in addition to the reflection color shift, more fantastic applications based on multiple optical parameter modulations can be reasonably anticipated.

3. Conclusion

This work presents a novel information-hiding and revealing method based on the asymmetric domain growth of BP I. When cooling under a temperature gradient, polydomain BP I is formed, leading to a complete hiding of the encoded information. After LCs reassembled from the homeotropic state with the aid of an electric field, patterned BP I monodomain is generated, resulting in a clear display of the encoded information. Through

alternating the stimuli applied onto the photopatterned BPLC cell, the polydomain and monodomain reversibly grow, and thus bistable information hiding and revealing are dynamically presented. The proposed design not only enhances the visual quality of the encoded information but also enables an electric-driven shifting of the reflection band. This work addresses the limitations of existing photonic crystals and brings flexible functions and tunable working bands to enable active photonics crystals. It may open new avenues for applications in optical encryption and information security.

4. Experimental Section

Materials: All BPLC samples were composed of 52.0 wt.% nematic LC HTW114200-050 ($\Delta\epsilon$ = 10.9 at 1 kHz, 20 °C, NCLCP, China), 35.0 wt.% chiral dopant S811 (helical twisting power = 8.3 μm^{-1} at 30 °C, NCLCP, China), 4.0 wt.% monomer RM257 (NCLCP, China), and 4.0 wt.% 2-ethylhexyl acrylate (EHA, Sigma–Aldrich, USA). The photoalignment agent sulfonic azo dye SD1 (NCLCP, China) was dissolved in dimethylformamide (DMF, Sigma–Aldrich, USA) at a concentration of 0.3 wt.%. The temperature was precisely controlled by a heating stage (LTS 120, Linkam, UK).

Cell Fabrication: ITO glass substrates were ultrasonically bathed and sequentially cleaned with UV–ozone. The bottom substrate was spin-coated with SD1 and then sealed with an untreated top substrate by epoxy glue mixed with 8 µm spacers to form a cell. The photopatterning was performed with a digital micromirror device (DMD)-based projection system (NCLCP, China).

Characterizations: Textures and Kossel diagrams were captured with two polarization optical microscopes (Nikon 50i, Japan, and Olympus BX51, Japan). All the reflection spectra were measured with a microscope spectrometer (PG2000-pro, Ideaoptics, China). A supercontinuum laser (SuperK EVO, NKT Photonics, Denmark) and a multichannel acousto-optic tunable filter (SuperK SELECT, NKT Photonics, Denmark) were used as light sources. Holographic displays were projected onto a black screen and captured by a digital camera (EOS M, Canon, Japan). The electric signal was generated by a digital function generator (33522B, Agilent, USA) and then amplified by a voltage amplifier (2340, Keysight, USA).

Supporting Information

Supporting Information is available from the Wiley Online Library or from the author.

Acknowledgements

Q.C. and C.O. contributed equally to this work. The authors gratefully acknowledge the support of the National Key Research and Development Program of China (2022YFA1203700), the National Natural Science Foundation of China (NSFC) (T2488302, 62405127 and 62035008), the Natural Science Foundation of Jiangsu Province (BK20233001) and the Postdoctoral Fellowship Program of CPSF under Grant Number (GZC20240640).

Conflict of Interest

The authors declare no conflict of interest.

Data Availability Statement

The data that support the findings of this study are available from the corresponding author upon reasonable request.

Keywords

anti-counterfeiting, blue phase liquid crystals, light-matter interactions, self-assembly, soft matter photonics

Received: October 1, 2024
Revised: November 11, 2024
Published online: November 26, 2024

[1] a) L. Lu, C. Fang, L. Fu, S. G. Johnson, J. D. Joannopoulos, M. Soljačić, *Nat. Phys.* **2016**, *12*, 337; b) G. J. Tang, X. T. He, F. L. Shi, J. W. Liu, X. D. Chen, J. W. Dong, *Laser Photonics Rev.* **2022**, *16*, 2100300.
[2] a) X. Gu, Y. Liu, G. Chen, H. Wang, C. Shao, Z. Chen, P. Lu, Y. Zhao, *ACS Appl. Mater. Interfaces* **2018**, *10*, 33936; b) P. Wu, J. Wang, L. Jiang, *Mater. Horiz.* **2020**, *7*, 338.
[3] a) D. Ge, E. Lee, L. Yang, Y. Cho, M. Li, D. S. Gianola, S. Yang, *Adv. Mater* **2015**, *27*, 2489; b) Y. Wang, H. Cui, Q. Zhao, X. Du, *Matter* **2019**, *1*, 626.
[4] J.-M. Lourtioz, H. Benisty, V. Berger, J.-M. Gerard, D. Maystre, A. Tchelnokov, *Towards Nanoscale Photonic Devices*, Springer, Berlin, Germany **2008**.
[5] A. R. Parker, V. L. Welch, D. Driver, N. Martini, *Nature* **2003**, *426*, 786.
[6] P. Vukusic, J. Sambles, C. Lawrence, *Nature* **2000**, *404*, 457.
[7] A. Loyau, D. Gomez, B. Moureau, M. Théry, N. S. Hart, M. S. Jalme, A. T. D. Bennett, G. Sorci, *Behav. Ecol.* **2007**, *18*, 1123.
[8] S. B. Juhl, E. P. Chan, Y. H. Ha, M. Maldovan, J. Brunton, V. Ward, T. Dokland, J. Kalmakoff, B. Farmer, E. L. Thomas, *Adv. Funct. Mater.* **2006**, *16*, 1086.
[9] J. Teyssier, S. V. Saenko, D. Van Der Marel, M. C. Milinkovitch, *Nat. Commun.* **2015**, *6*, 6368.
[10] M. He, J. P. Gales, É. Ducrot, Z. Gong, G.-R. Yi, S. Sacanna, D. J. Pine, *Nature* **2020**, *585*, 524.
[11] M. Moirangthem, A. P. Schenning, *ACS Appl. Mater. Interfaces* **2018**, *10*, 4168.
[12] a) S.-U. Kim, Y.-J. Lee, J. Liu, D. S. Kim, H. Wang, S. Yang, *Nat. Mater.* **2022**, *21*, 41; b) S. Y. Lin, Y. Q. Tang, W. X. Kang, H. K. Bisoyi, J. B. Guo, Q. Li, *Nat. Commun.* **2023**, *14*, 3005; c) L. Wang, Q. Li, *Adv. Funct. Mater.* **2016**, *26*, 10.
[13] P. G. D. Gennes, J. Prost, *The Physics of Liquid Crystals*, 2nd ed., Oxford University Press, New York **1993**.
[14] K. Yin, Y. H. Lee, Z. He, S. T. Wu, *Opt. Express* **2019**, *27*, 5814.
[15] Q. M. Chen, H. C. Wang, G. Y. Wang, C. T. Xu, Q. G. Tan, W. Duan, Y. Q. Lu, W. Hu, *Appl. Phys. Lett.* **2023**, *123*, 251101.
[16] C. T. Xu, B. H. Liu, C. Peng, Q. M. Chen, P. Chen, P. Z. Sun, Z. G. Zheng, Y. Q. Lu, W. Hu, *Adv. Opt. Mater.* **2022**, *10*, 2201088.
[17] Y. S. Zhang, Z. Q. Wang, W. C. Chuang, S. A. Jiang, T. S. Mo, J. D. Lin, C. R. Lee, *ACS Appl. Mater. Interfaces* **2021**, *13*, 55550.
[18] a) P. Chen, L. L. Ma, W. Hu, Z. X. Shen, H. K. Bisoyi, S. B. Wu, S. J. Ge, Q. Li, Y. Q. Lu, *Nat. Commun.* **2019**, *10*, 2518; b) Q. M. Chen, C. T. Xu, X. Liang, W. Hu, *Adv. Quantum Technol.* **2023**, *6*, 2200153.
[19] a) D. C. Wright, N. D. Mermin, *Rev. Mod. Phys.* **1989**, *61*, 385; b) J. Liu, W. Z. Liu, B. Guan, B. Wang, L. Shi, F. Jin, Z. G. Zheng, J. X. Wang, T. Ikeda, L. Jiang, *Nat. Commun.* **2021**, *12*, 3477.
[20] Y. Z. Yang, X. Zhang, Y. H. Chen, X. Yang, J. Z. Ma, J. X. Wang, L. Wang, W. Feng, *ACS Appl. Mater. Interfaces* **2021**, *13*, 41102.
[21] X. W. Xu, Y. J. Liu, D. Luo, *IEEE Photonics J.* **2022**, *14*, 2227805.
[22] F. S. Meng, C. L. Zheng, W. J. Yang, B. Guan, J. X. Wang, T. Ikeda, L. Jiang, *Adv. Funct. Mater.* **2022**, *32*, 2110985.
[23] W. Y. Cao, A. Muñoz, P. Palffy-Muhoray, B. Taheri, *Nat. Mater.* **2002**, *1*, 111.
[24] S. Cho, M. Takahashi, J.-i. Fukuda, H. Yoshida, M. Ozaki, *Commun. Mater.* **2021**, *2*, 39.

[25] H. Claus, O. Willekens, O. Chojnowska, R. Dąbrowski, J. Beeckman, K. Neyts, *Liq. Cryst.* **2016**, *43*, 688.
[26] R. Suryantari, Y. H. Shih, Y. H. Shih, H. Y. Chen, C. S. Wu, C. Y. Huang, *Opt. Lett.* **2023**, *48*, 77.
[27] C. W. Chen, C. T. Hou, C. C. Li, H. C. Jau, C. T. Wang, C. L. Hong, D. Y. Guo, C. Y. Wang, S. P. Chiang, T. J. Bunning, I. C. Khoo, T. H. Lin, *Nat. Commun.* **2017**, *8*, 727.
[28] a) J. A. Martínez-González, X. Li, M. Sadati, Y. Zhou, R. Zhang, P. F. Nealey, J. J. de Pablo, *Nat. Commun.* **2017**, *8*, 15854; b) M. Wang, C. Zou, J. Sun, L. Y. Zhang, L. Wang, J. M. Xiao, F. S. Li, P. Song, H. Yang, *Adv. Funct. Mater.* **2017**, *27*, 1702261; c) E. Otón, P. Morawiak, K. Gaładyk, J. M. Otón, W. Piecek, *Opt. Express* **2020**, *28*, 18202; d) S. Liu, I. Nys, K. Neyts, *Adv. Opt. Mater.* **2022**, *10*, 2200711.
[29] Z. G. Zheng, C. L. Yuan, W. Hu, H. K. Bisoyi, M. J. Tang, Z. Liu, P. Z. Sun, W. Q. Yang, X. Q. Wang, D. Shen, *Adv. Mater.* **2017**, *29*, 1703165.
[30] H. Yoshida, J. Kobashi, *Liq. Cryst.* **1909**, *43*, 1909.
[31] Q. M. Chen, X. Y. Wang, C. T. Xu, H. C. Chu, H. G. Yu, C. Ouyang, Y. Lai, Z. G. Zheng, X. Liang, Y. Q. Lu, W. Hu, *Laser Photonics Rev.* **2024**, *18*, 2301283.
[32] V. Chigrinov, A. Muravski, H. S. Kwok, H. Takada, H. Akiyama, H. Takatsu, *Phys. Rev. E* **2003**, *68*, 061702.
[33] a) R. J. Miller, H. F. Gleeson, *J. Phys. II* **1996**, *6*, 909; b) D. Y. Guo, C. W. Chen, C. C. Li, H. C. Jau, K. H. Lin, T. M. Feng, C. T. Wang, T. J. Bunning, I. C. Khoo, T. H. Lin, *Nat. Mater.* **2020**, *19*, 94.
[34] R. W. Gerchberg, *Optik* **1972**, *35*, 237.
[35] a) Y. X. Zhang, H. Yoshida, F. Chu, Y. Q. Guo, Z. Yang, M. Ozaki, Q. H. Wang, *Soft Matter* **2022**, *18*, 3328; b) Y. Zhang, H. Yoshida, Q. H. Wang, M. Ozaki, *Appl. Phys. Lett.* **2023**, 122.
[36] W. Hu, J. Sun, Q. Wang, L. Y. Zhang, X. T. Yuan, F. W. Chen, K. Li, Z. C. Miao, D. K. Yang, H. F. Yu, H. Yang, *Adv. Funct. Mater.* **2020**, *30*, 2004610.
[37] J. J. Yang, W. D. Zhao, Z. Yang, W. L. He, J. X. Wang, T. Ikeda, L. Jiang, *ACS Appl. Mater. Interfaces* **2019**, *11*, 46124.
[38] X. Zhang, Y. Z. Yang, P. Xue, C. Valenzuela, Y. H. Chen, X. Yang, L. Wang, W. Feng, *Angew. Chem., Int. Ed.* **2022**, *61*, e202211030.
[39] T. H. Lin, D. Y. Guo, C. W. Chen, T. M. Feng, W. X. Zeng, P. C. Chen, L. Y. Wu, W. M. Guo, L. M. Chang, H. C. Jau, C. T. Wang, T. J. Bunning, I. C. Khoo, *Nat. Commun.* **2024**, *15*, 7038.